On the Optical Properties of Diamino-Pillared Graphene Architectures

Emilia Papasouli, Nicolás Otero, Jacques Desmarais, Hassan Denawi, Demetrios Xenides, Emmanuel Klontzas, Emmanuel . Koukaras, Panaghiotis Karamanis

ON THE OPTICAL PROPERTIES OF DIAMINO-PILLARED GRAPHENE ARCHITECTURES.

Journal:	*The Journal of Physical Chemistry*
Manuscript ID	Draft
Manuscript Type:	Article
Date Submitted by the Author:	n/a
Complete List of Authors:	Papasouli, Emilia; Aristotle University of Thessaloniki, Chemistry Otero-Martnez, Nicolas; Departamento de Química Física, Facultade de Química, Universidade de Vigo, 36310 Vigo, Galicia, Spain Desmarais, Jacques; University of Turin, Chemistry Denawi, Hassan; Centre d'Élaboration de Matériaux et d'Études Structurales, Xenides, Demetrios; High School of Oinousses, Oinousses, 82101, Greece Klontzas, Emmanuel; National Hellenic Research Foundation, Theoretical and Physical Chemistry Institute Koukaras, Emmanuel; Aristotle University of Thessaloniki, School of Chemistry Karamanis, Panaghiotis; Institut des Sciences Analytiques et de Physico-chimie pour l'Environnement et les Materiaux,

ON THE OPTICAL PROPERTIES OF DIAMINO-PILLARED GRAPHENE ARCHITECTURES.

Emilia Papasouli,[a] Nicolás Otero,[b] Jacques Desmarais,[c] Hassan Denawi,[d] Demetrios Xenides,[e] Emmanuel Klontzas,[f] Emmanuel N. Koukaras,[a] Panaghiotis Karamanis*[d]

[a] Laboratory of Quantum and Computational Chemistry, Department of Chemistry, Aristotle University of Thessaloniki, 54124 Thessaloniki, Greece

[b] Department of Physical Chemistry, University of Vigo, Lagoas-Marcosende s/n, 36310.Vigo, Spain

[c] Dipartimento di Chimica, Universita di Torino, Via Giuria 5, 10125 Torino, Italy.

[d] E2S UPPA, CNRS, IPREM, Université de Pau et des Pays de l Adour, 64053 Pau, France

[e] High School of Oinousses, Oinousses, 82101, Greece

[f] Theoretical and Physical Chemistry Institute, National Hellenic Research Foundation, GR-116 35 Athens, Greece

*Corresponding author: P. Karamanis: panagiotis.karamanis@univ-pau.fr

Nicolás Otero: ORCID: 0000-0002-5313-7970

Abstract

Pillared graphenes are stacked graphene layers separated by spacers, or "pillars," of various types and have attracted significant attention in material science. In graphene networks, the pillars are used to increase interlayer distances and control their electronic conductivity, mechanical strength, and chemical reactivity. Such materials are currently investigated for a wide range of potential applications, including optoelectronics, flexible electronics, energy storage, catalysis, and sensing. In this work, we deal with the optical behavior of a special class of these promising materials in which graphene sheets, piled one on top of the other, are covalently connected by diamino organic molecules via carbon-nitrogen single bonds. In particular, we studied elemental molecular quantities strongly related to molecules and materials' linear and nonlinear optical profiles. Properties such as optical gaps, UV-Vis absorption spectra, excited states, and the first dipole hyperpolarizabilities have been computed and analyzed within the density functional theory (DFT) framework. The obtained results suggest that both the linear and the nonlinear optical profiles of graphene architectures interconnected by conventional organic diamino molecules are dominated by the optical responses of the graphene layers. On the other hand, the diamino pillars are indirectly involved, in the optical behavior of these species, through local structural modifications on the framework of the graphene sheets as a result of the cross-linking process. Specifically, the performed computations, conducted in large finite graphene flakes of specific aromaticity patterns, exposed that local structural patterns may trigger surprisingly strong variations with respect to their optical absorption profiles, excited states, and nonlinear optical behavior. Such local structural patterns involve *intercyclic* carbon-carbon single bonds formed between sp^3 hybridized carbon atoms belonging to two neighboring aromatic sextets. As far as the nonlinear optical properties are concerned, Kohn-Sham coupled perturbed computations on systems of various cross-linking patterns showed that NLO-inactive graphene sections, in terms of quadratic nonlinear optical responses, could be converted to materials of important nonlinearities. Finally, no evident dependence of the optical absorption profiles was observed with respect to the type (aromatic, conjugated or fully saturated) of the pillar used.

1. Introduction

During the past few years there has been an increasing interest in materials built from graphene sheets covalently interconnected by organic molecules. This class of multilayer graphenes, combine large interlayer distances and strong resistance against interlayer sliding with most of the extraordinary qualities of 2D-graphene[1–4] in terms of mechanical strength, elasticity, and electric/thermal conductance. Therefore, various types of pillared graphenes (PG) crosslinked by a great assortment of organic molecules (hereafter pillars) are currently synthesized and tested for applications ranging from fuel-gas and ion storage,[5,6,7–9] to molecular filtering.[10] Besides the interesting structural and mechanical features offered by PGs, it has also been reported[11,12] that the molecular pillars, covalently attached between two graphene sheets may alter the character of the overall electronic structure of the final material. As a result, pillar engineering could be employed to modify and eventually control useful electronic features such as their bandgap properties. Upon success in preparing PGs in a fully controlled manner, it is believed that this type of graphene networks might become strong candidates in technologies in which tunable band gaps and high degrees of mechanical strength/flexibility, are highly required as for instance in the realm of stretchable and wearable electronics[13–15]. This aspect of PGs has been predicted by some early theoretical simulations performed by Zhu *et al.* [11] on a series of graphene sheets covalently pillared with boronic acid. These authors provided numerical evidence demonstrating a direct link between band gaps and pillar type or density. In the same subject, recent Tight-Binding Density Functional computations conducted by Klontzas *et al.*[12] in a wider variety of covalently PGs, exposed an additional parameter on which the band gaps of such systems should depend on. This is the pillar distribution which seemed to have an important impact on the observed band gap variations.

Bearing in mind that graphene band gap engineering is of paramount importance for the integration of this material in current optoelectronic technologies, in this article we extend the above studies by investigating the optical properties[16] and behavior of such pillared networks. Our motive stems from the proven[17–27] potential of graphene materials to be implemented in technologies related to the photonics industry[28] that depends on materials allowing to efficiently control light with light.[29] In this work we mainly focus on PG architectures covalently interconnected by diamino organic molecules. Such systems are currently synthesized[30,31] and characterized with respect to their structures and reactivity. Among the successful reported works in the synthesis of covalently crosslinked graphenes we highlight the graphene-oxides interconnected by diaminoalkanes, synthesized by Herrera-Alonso *et al.*[32] that is one of the first articles in the subject. Also, we underline the works of Hung *et al.*[10] , Banda *et al.* [8] and Zhang *et al.*[6] who succeeded in "stitching" together layers of graphene oxide using simple organic molecules such as ethylene diamine, butylenediamine, and *p*-phenylenediamine as pillars.

The properties to be investigated in the following pages comprise optical gaps and UV-Vis absorption spectra together with fundamental molecular quantities strongly related to the optical behavior of molecular systems. Specifically, we examine ground state molecular dipole moments (μ_α), polarizabilities ($\alpha_{\alpha\beta}$), and first dipole hyperpolarizabilities ($\beta_{\alpha\beta\gamma}$) of pillared graphenes of finite size. These quantum quantities are met in the following (contracted to significant numerical terms) Taylor expansion series[33,34,35] [16]

$$\Delta\mu_\alpha = \mu_\alpha(F_a) - \mu_\alpha^0 = \alpha_{\alpha\beta}F_\beta + \frac{1}{2}\beta_{\alpha\beta\gamma}F_\beta F_\gamma + \frac{1}{6}\gamma_{\alpha\beta\gamma\delta}F_\beta F_\gamma F_\delta ...\#(1)$$

describing the induced molecular dipole dependence ($\Delta\mu_\alpha$) on external static electric fields (F). In brief, μ_α^0 is the permanent molecular dipole moment, $\alpha_{\alpha\beta}$ is the dipole polarizability, and $\beta_{\alpha\beta\gamma}$ is the first dipole hyperpolarizability, also referred to as second-order nonlinear polarizability, while $\gamma_{\alpha\beta\gamma\delta}$ is the second order dipole hyperpolarizability. Einstein summation has been used over repeated Cartesian indices α β and γ.

The molecular dipole polarizabilities, in general, are associated with the electron distribution in a molecule or atom. Molecules or atoms with more electrons or with electrons distributed farther from the nucleus are generally characterized by large polarizabilities. From another point of view, the dipole polarizability is related to molecular electron[36]density "softness" or "hardness" in response to external electric fields. The linear polarizabilities are also associated with light absorption spectra, Raman intensities, HOMO–LUMO gaps, and electronic excited states.[37] On the other hand, molecular first dipole hyperpolarizabilities are related to the nonlinear field-induced response of the electron cloud to an applied external electric field. Thus, while dipole polarizabilities express the ability of a material to undergo a polarization that is linearly proportional to the strength of the applied field, the first dipole hyperpolarizability measures the ability of a material to produce polarization proportional to its square. This molecular property is a key factor in fundamental processes in the realm of nonlinear optics,[16] as for instance, the process of second harmonic generation (SHG) in which two photons of the same frequency ω are combined within a material to produce light with frequency 2ω. The latter effect is one of the most iconic nonlinear optical effects related to the first-order dipole hyperpolarizability, currently applied in technologies varying from molecular spectroscopy[38] and bioimaging[39] to quantum optics and the generation of entangled photon pairs[40,41] with potential applications in quantum cryptography[42] and teleportation.[43]

As far as graphene is concerned, among the various NLO applications studied so far, those related to the cubic nonlinear responses ($\gamma_{\alpha\beta\gamma\delta}$) have captured most of the attention.[44–47] On the other hand, NLO experiments focusing on the second-order (or quadratic) responses have not been developed to the same extent in graphenes due to the centrosymmetric character of their structures which prohibits such nonlinear optical interactions between light and matter. As a result, most of the reported studies targeted on noncentrosymmetric edge functionalization[48–52] and in-plane doped graphene and graphene oxide

systems.[17,53–55] From this point of view, this piece of work provides, for the first time, handy estimations about the prospect of enabling second order NLO responses in graphene-based systems by "stitching" together with organic molecules quadratically inactive graphene sections.

2. Computational Details.

The coupled perturbed approximation[56–58] for finite and periodic systems[59–61] has been applied to calculate static dipole polarizabilities and first hyperpolarizabilities throughout this study. We relied on the Coulomb-attenuating (CAM-B3LYP)[62] functional that provides a good ratio between accuracy and computational efficiency for molecular nonlinear optical properties.[17,63] More information about nonlinear optical materials, the quantum-chemical nature of these universal material properties, and the computational methods that are frequently used for their accurate calculation can be found in standard books and articles (see refs [[64],[65–67]] and references therein).

Excited state properties for systems considered have been computed using the time-dependent DFT (TD) CAM-B3LYP method. The excited states of interest have been analyzed by means of natural transition orbitals[68] (NTOs) in terms of "excited particle" to "empty hole" of the electronic transition density matrix. For the optimization of the nuclear positions of the systems considered we used the parameter-free global-hybrid by Adamo and Barone,[69] widely referred to as PBE0. Also in this work, we computed six-center delocalization indices (*6*-DIs) accounting for the multicenter electron delocalization and aromaticity[70] via a Mulliken-based scheme within the Generalized Population Analysis (GPA).[71] All hyperpolarizability and excited state computations of finite and periodic systems have been carried out with GAUSSIAN16[72] and CRYSTAL17[73] suites of programs, respectively.

3. Results and Discussion

3.1 Molecular structures of pillared graphene models.

To facilitate the analysis of the linear and nonlinear optical properties of systems of such structural complexity, we initially applied our computational strategy to prototype highly symmetric finite models of purposely chosen cross-linking patterns. Specifically, we have considered five models of double-layered graphene flakes (PGFs) interconnected with six 1,4-benzenediamine pillars, as shown in **Figure 1.** Nomenclatures of pillared graphene **flakes (PGFs)** and illustrations of the corresponding cross-linking patterns. All PGFs share the same top flake. Each PGF is named as a function to the cross-linking pattern of its bottom flake as **(1, 2)- (α, β, γ)** and with respect to the chosen functionalization with **(H, OH)**. Description: "**1**", "**2**" denote sp^3 hybridized C atoms of the bottom flakes

bonded to one N atom of the p-diaminophenyl pillar at a specific position (**1**, **2**) as shown in the figure; "**α**,**"** "**β**,**"** and "**γ"** denote sp^3 hybridized C atoms of the bottom flakes functionalized with X= (H or OH) as shown in **Fig. 2.** Example: **1α-(OH)**: the nitrogen atom of the diamine pillar is bonded to the carbon atom "**1**", with a hydroxyl (**-OH)** bonded to the carbon atom at position "**α**."

All PGF models presented in that scheme are composed of two identical "claromatic" graphene armchair flakes (C_{114}) built from 114 carbon atoms, each. By the term "claromatic",[74,75] we refer to nanographene structures admitting solely one Clar [75–78] aromatic structure without any double bonds.

Previous experimental studies[79,80,81,82] suggest that diamine anchoring on graphene oxide (GO) is achieved by the reaction of the amino groups with epoxy sites (–C–O–C–) located in the framework of GO (see **Figure 2**). To be consistent with the respective reaction mechanism, we added the required –OH groups in trans positions in all symmetry-nonequivalent carbon atoms (labeled as **α**, **β**, and **γ)** that are bonded to each carbon atom chosen to play the role of nitrogen binding site. In addition, we have chosen to alternate –OH groups and nitrogen binding sites in a symmetric fashion, building initial PGF scaffolds of C_{6v} symmetry. The principal C_6 symmetry axes of their unrelaxed configurations have been set perpendicular to the molecular planes of the interconnected flakes passing through their centers of mass. To check for substitutional effects related to the presence of –OH groups, we increased the number of the systems from five to ten by considering an additional set of PGF models in which all –OH groups have been replaced by –H.

Geometry relaxations with tight convergence criteria, and no symmetry constraints of all ten systems considered at PBE0/def2-SVP level of theory, yielded real minima of C_1 symmetry. To obtain a measure of the final geometry distortions, we computed the nearest high point group symmetry of each configuration. The respective results revealed that cross-linking patterns **1α** and **2β** are close to the C_3 point group with a standard deviation below 0.01 Å. On the other hand, the remaining configurations were found very close to the C_6 symmetry with a standard deviation lower than 0.01 Å. Hence, none of the systems considered had the direction of their C_n symmetry axis seriously altered. This is confirmed by the dipole moment vectors, shown in **Figure 3**, which remained quasi-perpendicular to the planes of the pillared flakes as in their initial configurations of C_{6v} symmetry, regardless of the cross-linking pattern and the functionalization of each PGF. In contrast, the two latter features proved to be crucial for the scalar values and the direction (upward or downward) of the PGF electric dipole moments shown in **Figure 3**, which exhibit a strong dependence on either the binding sites of the pillars or on the functional group bonded to their neighboring carbon atoms.

3.2 Absorption spectra, HOMO-LUMO/Optical Gaps and Projected Densities of States

In **Figure 4a,** we present the cross-linking effect on the UV-Vis absorption simulated spectra with respect to the spectrum of the pristine dimer $(C_{114})_2$. For this task, we chose a "window" of ninety singlet ground to excited states quantum transitions. The obtained results demonstrate that the interconnection of the two identical armchair hexagonal flakes of D_{2h} symmetry with six *para*-benzenediamine pillars gives rise to broader, blue-shifted spectra with respect to their unpillared parent dimer. Hence, while the highly symmetric $(C_{114})_2$ dimer is predicted to feature one degenerated intense absorption band at 2.9 eV, its pillared derivatives tend to adopt two distinguishable bands of lower intensities stemming from the obvious symmetry breaking after geometry relaxations with no symmetry constraints. To rationalize the cross-linking effect on the electronic structures of these binary systems, let us start by comparing HOMO–LUMO (HL) and optical gaps of the modeled PGFs with those of the "non-pillared" parent $(C_{114})_2$ dimer. At first glance, the gap values presented in **Figure 4b** quickly reveal that the interconnection of the two C_{114} flakes with 1,4-benzenediamine linkers systematically results in smaller HL and optical gaps stemming from destabilizations of both HOMO and LUMO. The observed gap lowering is further justified by the inverse evolution of the polarizabilities per atom (also given in **Figure 4a),** which[36] are inversely proportional to the optical gaps of a given molecule by definition.[35] Hence, those PGFs featuring smaller HL and optical gaps are also characterized by the larger polarizabilities per atom.

More enlightening information about the band gap atomic contribution in these finite models has been obtained by studying the density of states of each system projected on the three fragments: a) the atoms of the pillars, b) the carbon centers of the bottom flakes, and c) the top flakes. A representative example of this analysis is provided in **Figure 5** in the case of PGFs **2β-H** and **2γ-H**. As seen, the global PGF HL gaps coincide with the "partial" gap of one out of the two pillared flakes. This outcome is further supported by the results presented in **Figure 6a**, where we compare the HL gaps of all pillared binary systems with X=H to those of non-pillared monolayer graphene flakes (GF) functionalized with $–NH_2$, as in their pillared counterparts. The computed values expose that all PGFs feature HL gaps lying very close to those of the isolated functionalized flake with the narrowest energy difference between their occupied and unoccupied orbitals. Similar behavior is obtained for the PGF functionalized with –OH (**Figures S1 and S2**). To obtain more insights into the optical properties of the considered PGF models, we performed a detailed analysis of those excited states which are involved in the most intense absorption bands of the PGF shown in **Figure 4**. The respective investigation, conducted by means of natural transition orbitals, suggested that both dominant absorption peaks are related to local intra-flake quantum transitions (**Figure S3**).

An additional significant trend that becomes evident from the above structure-property correlations concerns the weak influence of the pillars on the HL gaps of these systems. Such a tendency has been also observed in three-dimensional pillared graphene architectures by Klontzas *et al.*[12] Our results confirm and extend their conclusions to the optical absorption profiles of such systems. See, for instance, the results presented in **Figure 7,** where we compare the optical gaps and absorption profiles of pillared graphene flakes cross-linked by various molecules of different electron delocalization features (e.g., aromatic, conjugated, saturated hydrocarbons). The illustrated values show beyond any doubt that the type of diamine pillar marginally affects the linear optical behavior of the pillared dimers. This should not be surprising, bearing in mind that the HOMOs (LUMOs) of the pillars we considered are lying noticeably lower (higher) in energy than those of the interconnected flakes. Therefore, only pillars bearing similar HOMO and/or low LUMO energies with respect to the frontier orbital energies of graphene flakes could potentially influence the global optical behavior of these species.

3.3 Local structural features

To discuss the effect of local structural features on the optical properties of the PGF models considered in this work, we chose to start from the property variations presented in Figure **8a.** Thereby, we compare the HL and optical gaps of three groups of PGFs. The first group (group A) comprises structures **2α, 2β,** and **2γ** -(H) containing twelve sp^3 atoms in each GF. Starting from group A, we constructed an additional group of models (group B) by removing three out of the six pillars on each PGF. To maintain the sp^3 character of the corresponding binding carbon atoms, we added a hydrogen atom in each binding position. Therefore, group **B** comprises structures of three pillars and six sp^3 atoms on each flake. Finally, the third group (group **C**) has been built upon the structures of group **B** by converting the non-pillared sp^3 hybridized carbon atoms to sp^2.

A careful inspection of the gap evolution depicted in **Figure 8a** reveals a strong correlation between computed HL and optical gaps of a series of PGF systems and the presence of sp^3 hybridized carbon atoms in their frameworks. PGFs of the same number of sp^3 carbons (groups **A** and **B**) appear to feature similar optical gaps even if they are cross-linked by a smaller number of ligands. In contrast, PGFs of reduced numbers of sp^3 hybridized carbon atoms (group **C**) are characterized by profoundly wider optical gaps than the former. The only exception is observed in structure 1**α**-(H), for which the optical gap does not show a substantial dependence on the number of sp^3 carbon atoms. This is the only PGF of the five considered in which the diamine pillars bind to terminal aromatic rings which are bonded to more than two hydrogens. A more comprehensive picture demonstrating the dominant impact of the sp^3 carbons on the optical profiles of such double-layered systems is given in **Figure 8b**. Thereby, we contrast the UV-Vis spectra of some of

the pillared flakes of **Figure 1** to their non-pillared analogs functionalized with the same number of sp^3 carbon atoms lying on equivalent positions. It is more than obvious that both pillared and non-pillared species share similar optical profiles.

Let us focus on the most apparent quantitative aspects of the observed band gap changes. In that case, we see that out of the ten initial models considered intense HL-gap changes (> 1eV) are manifested only in PGFs 1**α**-H(OH) and 2**β**-H(OH). On the other hand, the gap modifications observed in the rest of the PGFs with respect to the interacting dimers are strikingly modest. This evident structure-property variation correlates with the electron delocalization results plotted in **Figure 6b.** Thereby, we have presented the aromaticity patterns of the flakes relying on computations of six-center π-electron delocalization in rings on the analog bottom single flake of each system functionalized with $–NH_2$ and –H. A careful inspection of those quantities exposes that out of the ten PGFs considered, 1**α**-H(OH) and 2**β**-H(OH) are the sole systems in which the nitrogen-bind sites and the sp^3 C–H carbons of the bottom flake, are lying on *intercyclic-single-bonds* connecting two neighboring aromatic sextets. Therefore, the delocalization distribution within each interconnected flake, as it is shaped after the crosslinking process, is most likely a decisive element on which the optical behavior of these systems depends on. This outcome might also be used to explain, up to a certain extent, the band gap dependence on the pillar distribution observed in periodic pillared graphene phases by Klontzas *et al*.[12]

3.4 Nonlinear optical properties

3.4.1 First hyperpolarizabilities.

Table 1 contains HLGs dipole moments, mean dipole polarizabilities, and tensorial components of the dipole hyperpolarizability of PGFs interconnected with diamino-benzene. We should remind here that the β_{xxx}, β_{yyy}, and β_{zzz} components express the nonlinear polarization capacity of a molecule along *x*, *y*, and *z* directions when an external electric field is applied on *x, y* and *z* molecular axes, respectively. In a similar manner, the tensorial component β_{xxz} expresses the "hyperpolarization" along Cartesian direction *x* and appears when two fields are applied to the *x and z* molecular axes. In addition, we have added the corresponding *β-modulus* [83]of the first hyperpolarizability ($\|\beta\|$) and indices $\Phi^{J=1}$ and $\Phi^{J=3}$, respectively, in the first-order nonlinear responses of these systems. All three quantities can be computed from the nonvanishing components of the tensor as follows:

$$\|\beta\| = \left[\beta_{xxx}^2 + \beta_{yyy}^2 + \beta_{zzz}^2 + 3(\beta_{xyy}^2 + \beta_{xzz}^2 + \beta_{yxx}^2 + \beta_{yzz}^2 + \beta_{zxx}^2 + \beta_{zyy}^2) + 6\beta_{xyz}^2\right]^{1/2} (2)$$

β-modulus reflects the "intrinsic" hyperpolarizability of any system, and it is used to compare first-order nonlinearities between molecules of varying symmetries. The respective expression is quite handy because it can be decomposed into two irreducible components as $\beta = \beta_{J=1} \oplus \beta_{J=3}$ or $||\beta_{J=1}||=[||\beta_{J=1}||^2+||\beta_{J=3}||^2]^{1/2}$. In the latter formula, $||\beta_{J=1}||$ represents the dipolar contributions while ($||\beta_{J=3}||$) stands for the octupolar contributions to the first hyperpolarizability. In terms of Cartesian tensorial β-components, the dipolar and octupolar components can be written as follows in conditions of Kleinman[84] symmetry:

$$\|\beta_{J=1}\| = \left[\frac{3}{5}\sum_i \beta_{iii}^2 + \frac{6}{5}\sum_{i\neq j}\beta_{iii}\beta_{ijj} + \frac{3}{5}\sum_{i\neq j}\beta_{ijj}^2 + \frac{6}{5}\sum_{i\neq j\neq k}\beta_{ijj}\beta_{ikk}\right]^{1/2} \quad (3)$$

$$\|\beta_{J=3}\| = \left[\frac{2}{5}\sum_i \beta_{iii}^2 - \frac{6}{5}\sum_{i\neq j}\beta_{iii}\beta_{ijj} + \frac{12}{5}\sum_{i\neq j}\beta_{ijj}^2 + \frac{6}{5}\sum_{i\neq j\neq k}\beta_{ijj}\beta_{ikk} + 6\sum_{i\neq j\neq k}\beta_{ijk}\right]^{1/2} \quad (4)$$

Using the above quantities, in which *i*, *j*, and *k* refer to Cartesian molecular directions *x*, *y*, and *z*, one can calculate the so-called nonlinear anisotropy parameter $\psi = \frac{\|\beta_{J=3}\|}{\|\beta_{J=1}\|}$ representing a measure of the interplay between the octupolar/dipolar contributions[85,86] on the first hyperpolarizability tensor β using the quantities $\Phi^{J=3} = \frac{\psi}{(\psi+1)}$ (octupolar contributions) and $\Phi^{J=1} = 1 - \Phi^{J=3}$ (dipolar contribution), respectively. Systems of strong octupolar contributions imply[83] strong couplings between exited states, while in systems where the dipolar contributions are more pronounced, prevailing ground-to-excited states transitions, should be expected, as in the case of long-established push-pull chromophores[35]. In the latter, the dominant first hyperpolarizability contributions come from charge-transfer excitations along the direction of their dipole moment, while in the former, the prevailing "hyperpolarization" mechanism also involves two-photon excitation paths occurring between virtual excited states connected by strong transition dipoles.[17]

The hyperpolarizability computations presented in **Table 1** have been conducted not only on the exact true minima of C_1 symmetry, obtained via full geometry relaxations, but also on configurations purposely symmetrized to the nearest highest symmetry point groups C_3 and/or C_6. Noncentrosymmetric molecules belonging to the latter symmetries must feature one dipole moment and two polarizability-independent components, respectively. In addition, they must carry four and two nonvanishing first hyperpolarizability independent tensorial components, respectively. For the molecular orientations shown in **Figure 3**, the nonvanishing components of the properties of interest are: $C_3 \equiv \mu_z$, $a_{xx}=a_{yy}$, a_{zz}, $\beta_{xxx}=-\beta_{xyy}$, $\beta_{yyy}=-\beta_{xxy}$, β_{zzz}, $\beta_{xxz}=\beta_{yyz}$ and $C_6 \equiv \mu_z$, $a_{xx}=a_{yy}$, a_{zz}, $\beta_{xxz}=-\beta_{yyz}$, β_{zzz}.

Bearing the above symmetry rules in mind, lets us now focus on the outcomes listed in **Table 1**. Starting from the *β-modulus*, one can easily distinguish PGFs **1α-H** and **1β-H** as the most hyperpolarizable species out of the five H-PGFs studied here. In their C_1 or C_3 symmetry configuration, these two PGFs carry strong first-dipole hyperpolarizabilities of more than 10×10^3 au. The computed $\Phi^{J=3}$ ($\Phi^{J=1}$) indices of 0.97 (0.3) for **1α-H-**C_3 and of 0.78 (0.22) for **1β-H-**C_3 point out that their first order nonlinearities should be of octupolar character owed to the strong in-plane β_{xxx} and β_{yyy} components. On the other hand, the contribution of the β_{zzz} components, related to polarization effects along the direction of their permanent dipole moments, is found relatively weak for **1a-H** (β_{zzz}=473 au) but considerably stronger for **2β-H** (β_{zzz}=1915 au).

The observed component variations are in line with the excited states discussed in a previous section. They indicate that the predicted strong nonlinearities should be credited more to *intra-flake* electronic excitations occurring within the top and/or bottom flakes than to *inter-flake* charge-transfer interactions. This is also implied by the weak β_{zzz} perpendicular components observed in PGFs apart from **2β-H**, which is related, though, to charge-transfer interactions between the p-diaminophenylene pillar and the bottom flake. To identify which of the two pillared graphene flakes contributes the most in large hyperpolarizabilities of **1α-H** or **2β-H** PGFs we computed the respective quantities of the isolated top and bottom graphene flakes functionalized with -H and -NH_2 groups illustrated in **Fig. 6.** As in the case of the HL-gaps, the obtained results clearly point out that the large hyperpolarizabilities of either **1α-H** or **2β-H** are similar in magnitudes with those of the non-pillared functionalized bottom flakes. For instance, the *β*-modulus computed for the isolated functionalized bottom flake of PGF **1α-H** is found to be only 1×10^3 au smaller than in its pillared counterpart (13×10^3 vs. 12×10^3 au, respectively).

Based on the inverse proportionality between the optical gap of a given system and its second order NLO responses,[17] one could initially deduce that the pronounced hyperpolarizabilities of **1α-H** and **2β-H** should mainly stem from their narrow band gaps, which in turn are defined by one of the two pillared flakes. However, computations conducted on fully symmetrized C_6 geometries of **1α-H** and **2β-H** PGFs**,** do not solely point to that end. For instance, in the case of **1α-H** PGF we see that the transition from C_3 symmetry to C_6 provokes a notable HL gap narrowing of 0.5 eV that could justify an increase in their first hyperpolarizabilities. In contrast, our calculations predict a threefold drop in the magnitude of modulus $||\beta||$ caused by the elimination of components β_{xxx} and β_{yyy} due to symmetry constraints. The analog behavior holds in the case of isomer **2β-H**. Therefore, the smaller gaps of either **1α-H** or **2β-H** should account only for a fourfold and fivefold difference, respectively, as compared to the rest of the isomers of this series of models.

In the case of the OH-functionalized PGFs, a similar behavior is observed. However, these species exhibit weaker hyperpolarizabilities than their hydrogenated counterparts. This is mainly due to a drastic reduction of the axial hyperpolarizability components along the *x* and *y* axes, occurring after replacing –H with –OH groups. To check whether the respective strong hyperpolarizability lowering is connected to substitution effects, we simply replaced all hydroxyl groups of **1α-OH** and **2β-OH** with H using a standard C–H bond length of 1.08 Å. Hyperpolarizability computations on unrelaxed structures of these systems revealed that modulus $||\beta||$ recovers a large portion of its strength after substituting OH with H. In brief, in the transition **1α(2β)-OH→1α(2β)-H** $||\beta||$ increased from 3.0×10^3 (4.9×10^3) to 10.3×10^3 (7.8×10^3) au, respectively. Consequently, the drastic reduction in the nonlinearities of the –OH functionalized models should be mainly attributed to effects related to the presence of –OH units in their framework via their implication in charge transfer transitions. From another viewpoint, the identified effects also imply that the NLO responses in such systems could be the subject of further modifications via the choice of functionalization agents.

In a previous section, we demonstrated that the choice of the pillar brings minor changes to the HL and optical gaps of the PGFs considered regardless of the cross-linking pattern. Let us now see if this is the case for the first order NLO responses of such systems, which from their definition, depend on a large set of quantum electronic transitions between the occupied and unoccupied molecular orbitals of a given NLO active species. For this task, we chose to present the results obtained on those patterns which yield the largest band gap variations within the series, designated by the prefixes **1α-** and **2β-**. At first glance, the hyperpolarizability results illustrated in **Figure 9** expose that intense modifications on the NLO capacity in such interconnected species are observed only in the case of diamino-butadiene. The analysis of the respective tensorial components suggests that the notable increase observed in the case of **1β-** patterns should be primarily attributed to the hyperpolarizability components parallel to the flake planes and secondarily to the perpendicular component of β tensor describing the nonlinear polarization along the C_3 symmetry axis of these systems which in this case are considerably strong. Nevertheless, the absence of such an effect in the case of cross-linking pattern **1a** indicates that the considerable property enhancement observed in this particular system should be more associated with its elaborated structure than with the pillar itself. Therefore, we will not further insist on discussing the source of this effect that depends on the relative alignment of the pillar's π valence orbitals and those of the bottom flake. Nonetheless, it is worth mentioning that this distinct outcome undoubtedly exposes the nontrivial electronic-structure character of pillared graphenes.

3.4.2 Pillared graphenes of enhanced NLO responses

The analysis of the static hyperpolarizabilities performed on purposely designed systems highlighted a distinct local structural pattern that appears to define the magnitudes of their first order NLO responses, which, in turn, depend on nontrivial transitions between more than one ground and excited states of a given system. The revealed pattern depends on the presence of sp^3 carbon atoms formed during the cross-linking process and on local electron delocalization features of the cross-linked graphene sections, which undergo drastic modifications with respect to the pristine case. Specifically, it was seen that the formation of intercyclic single bonds between sp^3 hybridized carbon atoms dramatically influences the band gaps of such systems and delivers large first-order nonlinearities. To test the robustness and limits of the observed structure-property correlations, we designed and performed the computational experiment described in **Figure 10(a)**. Thereby, we present hyperpolarizability results corresponding to four pairs of different PGFs interconnected with p-diaminophenyl pillars denoted as **1-(A, B) (–H, –OH)** and **2-(A, B)(–H, –OH)**. Note that in PGFs **2-(A, B)(–H, –OH)** species, the fully saturated C atoms are accommodated by a single aromatic hexagon. On the other hand, **1-(A, B) (–H, –OH)** both top and bottom flakes sp^3 carbon atoms have been placed on the heterojunctions of neighboring aromatic sextets. Based on the outcomes witnessed so far, we expect that this local structural feature appearing in both cross-linked flakes will deliver an increased NLO response. Computations at the CAM-B3LYP/def2-SVP level, schematically presented in **Figure 10,** fully confirm the last deduction. In addition, owing to their large number of electrons,[87–89] these species exhibit substantially strong second-order nonlinearities reaching orders of magnitude higher than 10^4 au maintaining wide optical gaps. If the latter feature is combined with the intense octupolar character of the overall responses, it leads to the conclusion that the strong NLO properties observed in these systems should involve strong excited state coupling.[17] Finally, a brief analysis of the first excited states of the considered propeller like PGFs confirmed that the transitions involved correspond to intra-flake electron density redistributions (**Figure S4**).

Finally, an approximate estimation about the size of the first order NLO magnitudes at the infinite periodic limit has been obtained by designing the periodic double-layer two-dimensional model of pillared graphene oxide shown in **Figure 10(b)**. The computed hyperpolarizability results (per unit cell) fully confirm the predictions obtained in finite systems about the capacity of such species to deliver extra strong (~10^7 au) first order NLO responses of octupolar character ($\beta^{J=3} \gg \beta^{J=1}$). In this case, the observed significant responses should be close to the nonzero but narrow band gap (~0.8 eV) obtained for this periodic infinite system. Interestingly, the projected density of states plotted in **Figure 10(b)** follows the trend according to which the global band gaps of pillared graphene architectures should be defined by the layer of the smallest energy gap between its valence and conduction bands.

4. Conclusions

Motivated by the recent advances in graphene materials, we conducted a systematic study on a series of properties related to the optical behavior of finite graphene sections covalently interconnected by diamino organic pillars. Our outcomes revealed that the linear and nonlinear optical behavior of such hybrid networks of nonzero band gaps is governed by the graphene fragments. Especially in the case of the nonlinear optical capacity of these systems, promising potential for applications related to technologies based on materials bearing high nonlinear optical coefficients has been identified. What's more, the performed analysis allowed us to spot intuitive local structural features that appear to play a decisive role in the observed property trends. Specifically, our computations revealed that *intercyclic* carbon-carbon single bonds formed between sp^3 hybridized carbon atoms belonging to two neighboring aromatic sextets are strongly related to drastic changes observed in the optical absorption profiles, excited states, and the nonlinear optical behavior of these species. As far as the pillars are concerned, in this work, we investigated conventional aromatic, conjugated, and fully saturated organic diamino molecules that have been used as pillars in several of the reported synthetic attempts. No noticeable property variations that could be related to their nature have been observed. We believe that pillars bearing similar HOMO and/or low LUMO energies with respect to the frontier orbital energies of graphene flakes could potentially influence the global optical behavior of these species. Finally, judging from the property differences observed between hydrogen and hydroxyl functionalized species, it became evident that further functionalization of the graphene layers could stimulate synergic effects between the pillars and the graphene sections.

5. Acknowledgments

Part of this work was granted access to the HPC resources of [CCRT/CINES/IDRIS] under the allocation 2022-2023 [AD010807031R1] made by GENCI (Grand Equipement National de Calcul Intensif). We also acknowledge the "Direction du Numérique" of the "Université de Pau et des Pays de l'Adour" for the computing facilities provided. Additional computing resources were provided by the High-Performance Computing Infrastructure of the Aristotle University of Thessaloniki (AUTh). AP thanks the "Pôle CAPT" of IPREM for the warm hospitality funded by ERASMUS+.

References

(1) Geim, A. K.; Novoselov, K. S. The Rise of Graphene. *Nat Mater* **2007**, *6* (3), 183–191. https://doi.org/10.1038/nmat1849.

(2) Castro Neto, A. H.; Guinea, F.; Peres, N. M. R.; Novoselov, K. S.; Geim, A. K. The Electronic Properties of Graphene. *Rev Mod Phys* **2009**, *81* (1), 109–162. https://doi.org/10.1103/RevModPhys.81.109.

(3) Novoselov, K. S.; Fal'ko, V. I.; Colombo, L.; Gellert, P. R.; Schwab, M. G.; Kim, K. A Roadmap for Graphene. *Nature* **2012**, *490* (7419), 192–200. https://doi.org/10.1038/nature11458.

(4) Novoselov, K. S.; Geim, A. K.; Morozov, S. v; Jiang, D.; Zhang, Y.; Dubonos, S. v; Grigorieva, I. v; Firsov, A. A. Electric Field Effect in Atomically Thin Carbon Films. *Science (1979)* **2004**, *306* (5696), 666–669. https://doi.org/10.1126/science.1102896.

(5) Bandyopadhyay, P.; Nguyen, T. T.; Li, X.; Kim, N. H.; Lee, J. H. Enhanced Hydrogen Gas Barrier Performance of Diaminoalkane Functionalized Stitched Graphene Oxide/Polyurethane Composites. *Compos B Eng* **2017**, *117*, 101–110. https://doi.org/10.1016/j.compositesb.2017.02.035.

(6) Zhang, B. M.; Zhang, Y. S.; Liu, M. C.; Li, J.; Lu, C.; Gu, B.; Liu, M. J.; Hu, Y. X.; Zhao, K.; Liu, W. W.; Niu, W. J.; Kong, L. bin; Chueh, Y. L. Chemical Welding of Diamine Molecules in Graphene Oxide Nanosheets: Design of Precisely Controlled Interlayer Spacings with the Fast Li+ Diffusion Coefficient toward High-Performance Storage Application. *Electrochim Acta* **2021**, *380*. https://doi.org/10.1016/j.electacta.2021.138114.

(7) Xie, Y.; Wang, X.; Hou, L.; Wang, X.; Zhang, Y.; Zhu, C.; Hu, Z.; He, M. Graphene Covalently Functionalized by Cross-Linking Reaction of Bifunctional Pillar Organic Molecule for High Capacitance. *J Energy Storage* **2021**, *38*. https://doi.org/10.1016/j.est.2021.102530.

(8) Banda, H.; Périé, S.; Daffos, B.; Taberna, P. L.; Dubois, L.; Crosnier, O.; Simon, P.; Lee, D.; de Paëpe, G.; Duclairoir, F. Sparsely Pillared Graphene Materials for High-Performance Supercapacitors: Improving Ion Transport and Storage Capacity. *ACS Nano* **2019**, *13* (2), 1443–1453. https://doi.org/10.1021/acsnano.8b07102.

(9) Banda, H.; Daffos, B.; Périé, S.; Chenavier, Y.; Dubois, L.; Aradilla, D.; Pouget, S.; Simon, P.; Crosnier, O.; Taberna, P. L.; Duclairoir, F. Ion Sieving Effects in Chemically Tuned Pillared Graphene Materials for Electrochemical Capacitors. *Chemistry of Materials* **2018**, *30* (9), 3040–3047. https://doi.org/10.1021/acs.chemmater.8b00759.

(10) Hung, W. S.; Tsou, C. H.; de Guzman, M.; An, Q. F.; Liu, Y. L.; Zhang, Y. M.; Hu, C. C.; Lee, K. R.; Lai, J. Y. Cross-Linking with Diamine Monomers to Prepare Composite Graphene Oxide-Framework Membranes with Varying d-Spacing. *Chemistry of Materials* **2014**, *26* (9), 2983–2990. https://doi.org/10.1021/cm5007873.

(11) Zhu, P.; Sumpter, B. G.; Meunier, V. Electronic, Thermal, and Structural Properties of Graphene Oxide Frameworks. *Journal of Physical Chemistry C* **2013**, *117* (16), 8276–8281. https://doi.org/10.1021/jp401072z.

(12) Klontzas, E.; Tylianakis, E.; Varshney, V.; Roy, A. K.; Froudakis, G. E. Organically Interconnected Graphene Flakes: A Flexible 3-D Material with Tunable Electronic Bandgap. *Sci Rep* **2019**, *9* (1), 13676. https://doi.org/10.1038/s41598-019-50037-y.

(13) Jo, J. W.; Lee, J. U.; Jo, W. H. Graphene-Based Electrodes for Flexible Electronics. *Polym Int* **2015**, *64* (12), 1676–1684. https://doi.org/10.1002/PI.4981.

(14) Jang, H.; Park, Y. J.; Chen, X.; Das, T.; Kim, M. S.; Ahn, J. H. Graphene-Based Flexible and Stretchable Electronics. *Advanced Materials* **2016**, *28* (22), 4184–4202. https://doi.org/10.1002/ADMA.201504245.

(15) Lim, S.; Son, D.; Kim, J.; Lee, Y. B.; Song, J.-K.; Choi, S.; Lee, D. J.; Kim, J. H.; Lee, M.; Hyeon, T.; Kim, D.-H. Wearable Electronics: Transparent and Stretchable Interactive Human Machine Interface Based on Patterned Graphene Heterostructures (Adv. Funct. Mater. 3/2015). *Adv Funct Mater* **2015**, *25* (3), 374–374. https://doi.org/10.1002/ADFM.201570020.

(16) Boyd, R. J.; Cheng Choi, S.; Hale, C. C. Electronic and Structural Properties of Borazine and Related Molecules. *Chem Phys Lett* **1984**, *112* (2), 136–141. https://doi.org/10.1016/0009-2614(84)85008-3.

(17) Karamanis, P.; Otero, N.; Pouchan, C. Unleashing the Quadratic Nonlinear Optical Responses of Graphene by Confining White-Graphene (h-BN) Sections in Its Framework. *J Am Chem Soc* **2014**, *136* (20), 7464–7473. https://doi.org/10.1021/ja502631w.

(18) Karamanis, P.; Otero, N.; Pouchan, C. Electric Property Variations in Nanosized Hexagonal Boron Nitride/Graphene Hybrids.*J Phys Chem C***2015**, *119* (21), 11872–11885. https://doi.org/10.1021/acs.jpcc.5b02793.

(19) Otero, N.; Pouchan, C.; Karamanis, P. Quadratic Nonlinear Optical (NLO) Properties of Borazino (B<inf>3</Inf>N<inf>3</Inf>)-Doped Nanographenes. *J Mater Chem C Mater* **2017**, *5* (32). https://doi.org/10.1039/c7tc01963g.

(20) Bao, Q.; Loh, K. P. Graphene Photonics, Plasmonics, and Broadband Optoelectronic Devices. *ACS Nano* **2012**, *6* (5), 3677–3694. https://doi.org/10.1021/nn300989g.

(21) Li, W.; Chen, B.; Meng, C.; Fang, W.; Xiao, Y.; Li, X.; Hu, Z.; Xu, Y.; Tong, L.; Wang, H.; Liu, W.; Bao, J.; Shen, Y. R. Ultrafast All-Optical Graphene Modulator. *Nano Lett* **2014**. https://doi.org/10.1021/nl404356t.

(22) Avouris, P. Graphene: Electronic and Photonic Properties and Devices. *Nano Lett* **2010**, *10* (11), 4285–4294. https://doi.org/10.1021/nl102824h.

(23) Xia, F.; Mueller, T.; Lin, Y.; Valdes-Garcia, A.; Avouris, P. Ultrafast Graphene Photodetector. *Nat Nanotechnol* **2009**, *4* (12), 839–843. https://doi.org/10.1038/nnano.2009.292.

(24) Koppens, F. H. L.; Mueller, T.; Avouris, Ph.; Ferrari, A. C.; Vitiello, M. S.; Polini, M. Photodetectors Based on Graphene, Other Two-Dimensional Materials and Hybrid Systems. *Nat Nanotechnol* **2014**, *9* (10), 780–793. https://doi.org/10.1038/nnano.2014.215.

(25) Yoneda, K.; Matsui, H.; Fukuda, K.; Takamuku, S.; Kishi, R.; Nakano, M. Open-Shell Characters and Second Hyperpolarizabilities for Hexagonal Graphene Nanoflakes Including Boron Nitride Domains. *Chem Phys Lett* **2014**, *595–596*, 220–225. https://doi.org/10.1016/j.cplett.2014.02.010.

(26) Yoneda, K.; Matsui, H.; Fukuda, K.; Takamuku, S.; Kishi, R.; Nakano, M. Open-Shell Characters and Second Hyperpolarizabilities for Hexagonal Graphene Nanoflakes Including Boron Nitride Domains. *Chem Phys Lett* **2014**, *595–596*, 220–225. https://doi.org/10.1016/j.cplett.2014.02.010.

(27) Yoneda, K.; Nakano, M.; Inoue, Y.; Inui, T.; Fukuda, K.; Shigeta, Y.; Kubo, T.; Champagne, B. Impact of Antidot Structure on the Multiradical Characters, Aromaticities, and Third-Order Nonlinear Optical Properties of Hexagonal Graphene Nanoflakes.*J Phys Chem C***2012**, *116* (33), 17787–17795. https://doi.org/10.1021/jp305171k.

(28) Bonaccorso, F.; Sun, Z.; Hasan, T.; Ferrari, A. C. Graphene Photonics and Optoelectronics. *Nature Photon.* **2010**, *4*, 611.

(29) Fainman, Y.; Ma, J.; Lee, S. H. Non-Linear Optical Materials and Applications. *Materials Science Reports* **1993**, *9* (2–3), 53–139. https://doi.org/10.1016/0920-2307(93)90008-3.

(30) Lee, K.; Yoon, Y.; Cho, Y.; Lee, S. M.; Shin, Y.; Lei, H.; Lee, H. Tunable Sub-Nanopores of Graphene Flake Interlayers with Conductive Molecular Linkers for Supercapacitors. *ACS Nano* **2016**, *10* (7), 6799–6807. https://doi.org/10.1021/ACSNANO.6B02415/SUPPL_FILE/NN6B02415_SI_001.PDF.

(31) Bandyopadhyay, P.; Nguyen, T. T.; Li, X.; Kim, N. H.; Lee, J. H. Enhanced Hydrogen Gas Barrier Performance of Diaminoalkane Functionalized Stitched Graphene Oxide/Polyurethane Composites. *Compos B Eng* **2017**, *117*, 101–110. https://doi.org/10.1016/j.compositesb.2017.02.035.

(32) Herrera-Alonso, M.; Abdala, A. A.; McAllister, M. J.; Aksay, I. A.; Prud'homme, R. K. Intercalation and Stitching of Graphite Oxide with Diaminoalkanes. *Langmuir* **2007**, *23* (21), 10644–10649. https://doi.org/https://doi.org/10.1021/la0633839.

(33) Buckingham, A. D. Permanent and Induced Molecular Moments and Long-Range Intermolecular Forces. In *Advances in Chemical Physics*; Hirschfelder, J. O., Ed.; John Wiley & Sons, Inc., 1967; pp 107–142.

(34) McLean, A. D.; Yoshimine, M. Theory of Molecular Polarizabilities. *J Chem Phys* **1967**, *47* (6), 1927–1935. https://doi.org/10.1063/1.1712220.

(35) Kanis, D. R.; Ratner, M. A.; Marks, T. J. Design and Construction of Molecular Assemblies with Large Second-Order Optical Nonlinearities. Quantum Chemical Aspects. *Chem Rev* **1994**, *94* (1), 195–242. https://doi.org/10.1021/cr00025a007.

(36) Otero, N.; Karamanis, P.; Pouchan, C. Hirshfeld-Based Atomic Population Analysis of the B, N Doping Effect in Zigzag Graphene Nanoribbons: π Electron Density as Requirement to Follow the B, N Doping Guidelines. *Theor Chem Acc* **2018**, *137* (2). https://doi.org/10.1007/s00214-017-2189-5.

(37) Albrecht, A. C. On the Theory of Raman Intensities. *J Chem Phys* **1961**, *34* (5), 1476–1484. https://doi.org/10.1063/1.1701032.

(38) Heinz, T. F.; Chen, C. K.; Ricard, D.; Shen, Y. R. Spectroscopy of Molecular Monolayers by Resonant Second-Harmonic Generation. *Phys Rev Lett* **1982**, *48* (7), 478. https://doi.org/10.1103/PhysRevLett.48.478.

(39) Chen, X.; Nadiarynkh, O.; Plotnikov, S.; Campagnola, P. J. Second Harmonic Generation Microscopy for Quantitative Analysis of Collagen Fibrillar Structure. *Nat Protoc* **2012**, *7* (4). https://doi.org/10.1038/nprot.2012.009.

(40) Zhao, J.; Ma, C.; Rüsing, M.; Mookherjea, S. High Quality Entangled Photon Pair Generation in Periodically Poled Thin-Film Lithium Niobate Waveguides. *Phys Rev Lett* **2020**, *124*, 163603. https://doi.org/10.1103/PhysRevLett.124.163603.

(41) Zhang, Z.; Yuan, C.; Shen, S.; Yu, H.; Zhang, R.; Wang, H.; Li, H.; Wang, Y.; Deng, G.; Wang, Z.; You, L.; Wang, Z.; Song, H.; Guo, G.; Zhou, Q. High-Performance Quantum Entanglement Generation via Cascaded Second-Order Nonlinear Processes. *npj Quantum Information 2021 7:1* **2021**, *7* (1), 1–9. https://doi.org/10.1038/S41534-021-00462-7.

(42) Gisin, N.; Ribordy, G.; Tittel, W.; Zbinden, H. Quantum Cryptography. *Rev. Mod. Phys.* **2002**, *74* (1), 145. https://doi.org/10.1103/revmodphys.74.145.

(43) Valivarthi, R.; Puigibert, M. G.; Zhou, Q.; Aguilar, G. H.; Verma, V. B.; Marsili, F.; Shaw, M. D.; Nam, S. W.; Oblak, D.; Tittel, W. Quantum Teleportation across a Metropolitan Fibre Network. *Nat. Photonics* **2016**, *10* (10), 676–680. https://doi.org/10.1038/nphoton.2016.180.

(44) Jiang, T.; Huang, D.; Cheng, J.; Fan, X.; Zhang, Z.; Shan, Y.; Yi, Y.; Dai, Y.; Shi, L.; Liu, K.; Zeng, C.; Zi, J.; Sipe, J. E.; Shen, Y.-R.; Liu, W.-T.; Wu, S. Gate-Tunable Third-Order Nonlinear Optical Response of Massless Dirac Fermions in Graphene. *Nat Photonics* **2018**, *12* (7), 430–436. https://doi.org/10.1038/s41566-018-0175-7.

(45) Zhang, M.; Li, G.; Li, L. Graphene Nanoribbons Generate a Strong Third-Order Nonlinear Optical Response upon Intercalating Hexagonal Boron Nitride. *J Mater Chem C Mater* **2014**, *2* (8), 1482–1488. https://doi.org/10.1039/C3TC31847H.

(46) Stavrou, M.; Papadakis, I.; Bawari, S.; Narayanan, T. N.; Couris, S. Giant Broadband (450–2300 Nm) Optical Limiting and Enhancement of the Nonlinear Optical Response of Some Graphenes by Defect Engineering.*J Phys Chem C***2021**, *125* (29), 16075–16085. https://doi.org/10.1021/acs.jpcc.1c05495.

(47) Mateo-Alonso, A.; Iliopoulos, K.; Couris, S.; Prato, M. Efficient Modulation of the Third Order Nonlinear Optical Properties of Fullerene Derivatives. *J Am Chem Soc* **2008**, *130* (5), 1534–1535. https://doi.org/10.1021/ja0771235.

(48) Yamuna, R.; Ramakrishnan, S.; Dhara, K.; Devi, R.; Kothurkar, N. K.; Kirubha, E.; Palanisamy, P. K. Synthesis, Characterization, and Nonlinear Optical Properties of Graphene Oxide Functionalized with Tetra-Amino Porphyrin. *Journal of Nanoparticle Research* **2013**, *15* (1), 1–9. https://doi.org/10.1007/s11051-012-1399-y.

(49) Zhang, X.; Yu, G.; Huang, X.; Chen, W. Introducing the Triangular BN Nanodot or Its Cooperation with the Edge-Modification via the Electron-Donating/Withdrawing Group to Achieve the Large First Hyperpolarizability in a Carbon Nanotube System. *Physical Chemistry Chemical Physics* **2017**, *19* (27), 17834–17844. https://doi.org/10.1039/C7CP02327H.

(50) Tian, P.; Tang, L.; Teng, K. S.; Xiang, J.; Lau, S. P. Recent Advances in Graphene Homogeneous p–n Junction for Optoelectronics. *Adv Mater Technol* **2019**, *4* (7), 1900007. https://doi.org/10.1002/admt.201900007.

(51) Ma, F.; Zhou, Z.-J.; Liu, Y.-T.; Zhang, Y.-Z.; Miao, T.-F.; Li, Z.-R. Substituted Graphene Nano-Flakes: Defective Structure and Large Nonlinear Optical Property. *Chem Phys Lett* **2011**, *504* (4–6), 211–215. https://doi.org/10.1016/j.cplett.2011.02.007.

(52) Zhang, X.-L.; Zhao, X.; Liu, Z.-B.; Liu, Y.-S.; Chen, Y.-S.; Tian, J.-G.; Hor, S. A.; Ji, W.; Broadband, ". *Enhanced Nonlinear Optical Properties of Graphene-Oligothiophene Hybrid Material*; 2009.

(53) Biswas, S.; Tiwary, C. S.; Vinod, S.; Kole, A. K.; Chatterjee, U.; Kumbhakar, P.; Ajayan, P. M. Nonlinear Optical Properties and Temperature Dependent Photoluminescence in HBN-GO Heterostructure 2D Material.*J Phys Chem C***2017**. https://doi.org/10.1021/acs.jpcc.6b12834.

(54) Zhang, Y.; Huang, D.; Shan, Y.; Jiang, T.; Zhang, Z.; Liu, K.; Shi, L.; Cheng, J.; Sipe, J. E.; Liu, W.-T.; Wu, S. Doping-Induced Second-Harmonic Generation in Centrosymmetric Graphene from Quadrupole Response. *Phys Rev Lett* **2019**, *122* (4). https://doi.org/10.1103/PhysRevLett.122.047401.

(55) Loh, K. P.; Bao, Q.; Eda, G.; Chhowalla, M. Graphene Oxide as a Chemically Tunable Platform for Optical Applications. *Nature Chemistry 2010 2:12* **2010**, *2* (12), 1015–1024. https://doi.org/10.1038/NCHEM.907.

(56) Hurst, G. J. B.; Dupuis, M.; Clementi, E. Ab Initio Analytic Polarizability, First and Second Hyperpolarizabilities of Large Conjugated Organic Molecules: Applications to Polyenes C 4H6 to C22H24. *J Chem Phys* **1988**, *89* (1). https://doi.org/10.1063/1.455480.

(57) Dykstra, C. E.; Jasien, P. G. Derivative Hartree—Fock Theory to All Orders. *Chem Phys Lett* **1984**, *109* (4), 388–393. https://doi.org/10.1016/0009-2614(84)85607-9.

(58) Gerratt, J.; Mills, I. M. Force Constants and Dipole-Moment Derivatives of Molecules from Perturbed Hartree-Fock Calculations. I. *J Chem Phys* **1968**, *49* (4), 1719–1729. https://doi.org/10.1063/1.1670299.

(59) Ferrero, M.; Ŕrat, M.; Orlando, R.; Dovesi, R. Coupled Perturbed Hartree-Fock for Periodic Systems: The Role of Symmetry and Related Computational Aspects. *Journal of Chemical Physics* **2008**, *128* (1). https://doi.org/10.1063/1.2817596.

(60) Ferrero, M.; Rérat, M.; Orlando, R.; Dovesi, R. The Calculation of Static Polarizabilities of 1-3D Periodic Compounds. the Implementation in the CRYSTAL Code. *J Comput Chem* **2008**, *29* (9). https://doi.org/10.1002/jcc.20905.

(61) Ferrero, M.; Rérat, M.; Kirtman, B.; Dovesi, R. Calculation of First and Second Static Hyperpolarizabilities of One- to Three-Dimensional Periodic Compounds. Implementation in the CRYSTAL Code. *J Chem Phys* **2008**, *129* (24), 244110. https://doi.org/10.1063/1.3043366.

(62) Yanai, T.; Tew, D. P.; Handy, N. C. A New Hybrid Exchange–Correlation Functional Using the Coulomb-Attenuating Method (CAM-B3LYP). *Chem Phys Lett* **2004**, *393* (1–3), 51–57. https://doi.org/10.1016/j.cplett.2004.06.011.

(63) Karamanis, P.; Otero, N.; Xenides, D.; Denawi, H.; Mandado, M.; Rérat, M. From Pyridine Adduct of Borabenzene to (In)Finite Graphene Architectures Functionalized with N → B Dative Bonds. Prototype Systems of Strong One- and Two-Photon Quantum Transitions Triggering Large Nonlinear Optical Responses.*J Phys Chem C***2020**, *124* (38), 21063–21074. https://doi.org/10.1021/acs.jpcc.0c05190.

(64) Papadopoulos, M. G.; Sadlej, A. J.; Leszczynski, J. *Non-Linear Optical Properties of Matter: From Molecules to Condensed Phases*; Springer Netherlands, 2006.

(65) Bishop, D. M.; Luis, J. M.; Kirtman, B. Vibration and Two-Photon Absorption. *J Chem Phys* **2002**, *116* (22), 9729–9739. https://doi.org/10.1063/1.1477179.

(66) Bishop, D.; Cheung, L. M.; Buckingham, A. D. Dipole Polarizability Formulae. *Mol Phys* **1980**, *41* (5), 1225–1226. https://doi.org/10.1080/00268978000103911.

(67) Bishop, D. M. Aspects of Non-Linear-Optical Calculations. In *Advances in Quantum Chemistry*; Zerner, J. R. S. and M. C., Ed.; Academic Press, 1994; Vol. 25, pp 1–45.

(68) Martin, R. L. Natural Transition Orbitals. *J Chem Phys* **2003**, *118* (11), 4775–4777. https://doi.org/10.1063/1.1558471.

(69) Adamo, C.; Barone, V. Toward Reliable Density Functional Methods without Adjustable Parameters: The PBE0 Model. *J Chem Phys* **1999**, *110* (13), 6158. https://doi.org/10.1063/1.478522.

(70) Giambiagi, M.; Giambiagi, M. S. de; Silva, C. D. dos S.; Figueiredo, A. P. de. Multicenter Bond Indices as a Measure of Aromaticity. *Physical Chemistry Chemical Physics* **2000**, *2* (15), 3381–3392. https://doi.org/10.1039/B002009P.

(71) Bultinck, P.; Ponec, R.; van Damme, S. Multicenter Bond Indices as a New Measure of Aromaticity in Polycyclic Aromatic Hydrocarbons. *J Phys Org Chem* **2005**, *18* (8), 706–718. https://doi.org/10.1002/poc.922.

(72) Frisch, M. J.; Trucks, G. W.; Schlegel, H. B.; Scuseria, G. E.; Robb, M. A.; Cheeseman, J. R.; Scalmani, G.; Barone, V.; Petersson, G. A.; Nakatsuji, H.; Li, X.; Caricato, M.; Marenich, A. v; Bloino, J.; Janesko, B. G.; Gomperts, R.; Mennucci, B.; Hratchian, H. P.; Ortiz, J. v; Izmaylov, A. F.; Sonnenberg, J. L.; Williams-Young, D.; Ding, F.; Lipparini, F.; Egidi, F.; Goings, J.; Peng, B.; Petrone, A.; Henderson, T.; Ranasinghe, D.; Zakrzewski, V. G.; Gao, J.; Rega, N.; Zheng, G.; Liang, W.; Hada, M.; Ehara, M.; Toyota, K.; Fukuda, R.; Hasegawa, J.; Ishida, M.; Nakajima, T.; Honda, Y.; Kitao, O.; Nakai, H.; Vreven, T.; Throssell, K.; Montgomery Jr., J. A.; Peralta, J. E.; Ogliaro, F.; Bearpark, M. J.; Heyd, J. J.; Brothers, E. N.; Kudin, K. N.; Staroverov, V. N.; Keith, T. A.; Kobayashi, R.; Normand, J.; Raghavachari, K.; Rendell, A. P.; Burant, J. C.; Iyengar, S. S.; Tomasi, J.; Cossi, M.; Millam, J. M.; Klene, M.; Adamo, C.; Cammi, R.; Ochterski, J. W.; Martin, R. L.; Morokuma, K.; Farkas, O.; Foresman, J. B.; Fox, D. J. Gaussian˜16 Revision C.01. 2016.

(73) Dovesi, R.; Erba, A.; Orlando, R.; Zicovich-Wilson, C. M.; Civalleri, B.; Maschio, L.; Rérat, M.; Casassa, S.; Baima, J.; Salustro, S.; Kirtman, B. Quantum-Mechanical Condensed Matter Simulations with CRYSTAL. *WIREs Computational Molecular Science* **2018**, *8* (4), e1360. https://doi.org/10.1002/wcms.1360.

(74) Balaban, A. T.; Klein, D. J. Claromatic Carbon Nanostructures.*J Phys Chem C***2009**, *113* (44), 19123–19133. https://doi.org/10.1021/jp9082618.

(75) Balaban, A. T.; Oniciu, D. C.; Katritzky, A. R. Aromaticity as a Cornerstone of Heterocyclic Chemistry. *Chem Rev* **2004**, *104* (5), 2777–2812. https://doi.org/10.1021/cr0306790.

(76) Randić, M. Aromaticity of Polycyclic Conjugated Hydrocarbons. *Chem Rev* **2003**, *103* (9), 3449–3606. https://doi.org/10.1021/cr9903656.

(77) Martín-Martínez, F. J.; Fias, S.; Van Lier, G.; De Proft, F.; Geerlings, P. Electronic Structure and Aromaticity of Graphene Nanoribbons. *Chemistry – A European Journal* **2012**, *18* (20), 6183–6194. https://doi.org/10.1002/chem.201103977.

(78) Otero, N.; El-kelany, K. E.; Pouchan, C.; Rérat, M.; Karamanis, P. Establishing the Pivotal Role of Local Aromaticity in the Electronic Properties of Boron-Nitride Graphene Lateral Hybrids. *Phys Chem Chem Phys* **2016**, *18* (36), 25315–25328. https://doi.org/10.1039/C6CP04502B.

(79) Tsoufis, T.; Tuci, G.; Caporali, S.; Gournis, D.; Giambastiani, G. P-Xylylenediamine Intercalation of Graphene Oxide for the Production of Stitched Nanostructures with a Tailored Interlayer Spacing. *Carbon N Y* **2013**, *59*, 100–108. https://doi.org/10.1016/j.carbon.2013.02.059.

(80) Wang, S.; Chia, P. J.; Chua, L. L.; Zhao, L. H.; Png, R. Q.; Sivaramakrishnan, S.; Zhou, M.; Goh, R. G. S.; Friend, R. H.; Wee, A. T. S.; Ho, P. K. H. Band-like Transport in Surface-Functionalized Highly

Solution-Processable Graphene Nanosheets. *Adv Mat* **2008**, *20* (18), 3440–3446. https://doi.org/10.1002/adma.200800279.

(81) Yang, H.; Shan, C.; Li, F.; Han, D.; Zhang, Q.; Niu, L. Covalent Functionalization of Polydisperse Chemically-Converted Graphene Sheets with Amine-Terminated Ionic Liquid. *Chem Comm* **2009**, No. 26, 3880–3882. https://doi.org/10.1039/b905085j.

(82) Vacchi, I. A.; Raya, J.; Bianco, A.; Ménard-Moyon, C. Controlled Derivatization of Hydroxyl Groups of Graphene Oxide in Mild Conditions. *2d Mater* **2018**, *5* (3). https://doi.org/10.1088/2053-1583/aac8a9.

(83) Zyss, J.; Ledoux, I. Nonlinear Optics in Multipolar Media: Theory and Experiments. *Chem Rev* **1994**, *94* (1), 77–105. https://doi.org/10.1021/cr00025a003.

(84) Kleinman, D. A. Nonlinear Dielectric Polarization in Optical Media. *Phys Rev* **1962**, *126* (6), 1977–1979. https://doi.org/10.1103/PhysRev.126.1977.

(85) Rodriguez, V.; Grondin, J.; Adamietz, F.; Danten, Y. Local Structure in Ionic Liquids Investigated by Hyper-Rayleigh Scattering. *J Phys Chem B* **2010**, *114* (46), 15057–15065. https://doi.org/10.1021/jp107165k.

(86) Castet, F.; Bogdan, E.; Plaquet, A.; Ducasse, L.; Champagne, B.; Rodriguez, V. Reference Molecules for Nonlinear Optics: A Joint Experimental and Theoretical Investigation. *J Chem Phys* **2012**, *136* (2), 024506. https://doi.org/10.1063/1.3675848.

(87) Zhou, J.; Kuzyk*, M. G. Intrinsic Hyperpolarizabilities as a Figure of Merit for Electro-Optic Molecules.*J Phys Chem C***2008**, *112* (21), 7978–7982. https://doi.org/10.1021/jp7120824.

(88) Kuzyk, M. G. Connecting at the Speed of Light. *IEEE Circuits and Devices Magazine* **2003**, *19* (5), 8–17. https://doi.org/10.1109/MCD.2003.1236782.

(89) Kuzyk, M. G. Physical Limits on Electronic Nonlinear Molecular Susceptibilities. *Phys Rev Lett* **2000**, *85* (6), 1218–1221. https://doi.org/10.1103/PhysRevLett.85.1218.

TABLES

Table 1. HOMO-LUMO gaps (HLG in eV), dipole moments (au), mean dipole polarizabilities (au), dipole hyperpolarizability (au) tensorial components, $\|\beta\|$ modulus (au), depolarization ratios (Ψ), octupolar ($\Phi^{J=3}$) and dipolar ($\Phi^{J=1}$) contributions of all PGFs interconnected with diamino-benzene fixed in C_3 and C_6 symmetries. Numbers in parenthesis correspond to property values computed on the exact equilibrium geometries of these species belonging to the C_1 symmetry

		Sym.	HLG	OPG	μ_z	a_{xx}	a_{zz}	$\overline{\alpha}\times10^3$	β_{xxx}	β_{yyy}	β_{xxz}	β_{zzz}	$\|\beta\|\times10^3$	Ψ	$\Phi^{J=3}$	$\Phi^{J=1}$
-H	**1α**	C_3	2.74(2.74)	(1.63)	1.0 (1.0)	4770	1427	3.7(3.7)	4809	4621	60	473	13.3 (13.4)	29.03	0.97	0.03
	1α	C_6	2.24	..	0.9	5055	1437	3.8	-	-	1616	277	4.0	1.06	0.52	0.48
	1β	C_6	3.64(3.65)	(2.00)	-0.2(-0.2)	4144	1439	3.2(3.2)	-	-	323	224	0.8 (0.8)	0.70	0.41	0.59
	2α	C_6	3.53(3.53)	(1.97)	1.7(1.7)	4210	1468	3.3(3.3)	-	-	258	258	0.8 (0.8)	14.73	0.94	0.06
	2β	C_3	2.38(2.38)	(1.16)	1.3(1.3)	4864	1475	3.7(3.7)	-4938	-1115	876	1915	10.5(10.8)	13.57	0.78	0.22
	2β	C_6	1.85	..	1.4	5296	1474	4.0	-	-	868	2460	4.8 (10.8)	0.45	0.31	0.69
	2γ	C_6	3.66 (3.66)	(2.39)	0.8(0.8)	4156	1468	3.3 (3.3)	-	-	-269	460	0.8 (0.8)	13.08	0.93	0.07
-OH	**1α**	C_3	2.98(2.99)	(1.70)	-0.6 (-0.7)	4695	1480	3.62 (3.6)	-744	-846	650	1252	3.0 (3.0)	1.16	0.54	0.46
	1α	C_6	2.12	..	-1.2	5198	1483	3.96	-	-	1112	1114	2.9	0.54	0.35	0.65
	1β	C_6	3.42(3.35)	(1.79)	-1.0 (-0.9)	4191	1485	3.29 (3.3)	-	-	380	349	1.0 (1.0)	0.58	0.37	0.63
	2α	C_6	3.37(3.37)	(1.76)	-0.2 (-0.2)	4255	1520	3.34 (3.3)	-	-	-80	1103	1.1 (1.1)	1.16	0.54	0.46
	2β	C_3	2.46(2.46)	(1.08)	-0.6 (-0.6)	4813	1524	3.71 (3.7)	619	-1695	868	2460	4.9 (5.0)	1.11	0.53	0.47
	2β	C_6	1.67	..	-0.6	5493	1525	4.2	-	-	790	2602	3.2	0.05	0.04	0.96
	2γ	C_6	3.65(3.65)	(2.36)	-0.4 (-0.4)	4180	1498	3.28 (3.3)	-	-	-192	852	1.0 (1.0)	2.49	0.71	0.29

point group. All property computations have been carried out at CAM-B3LYP/def2-SVP level of theory applied on PBE0/def2-SVP optimized geometries.

Figures

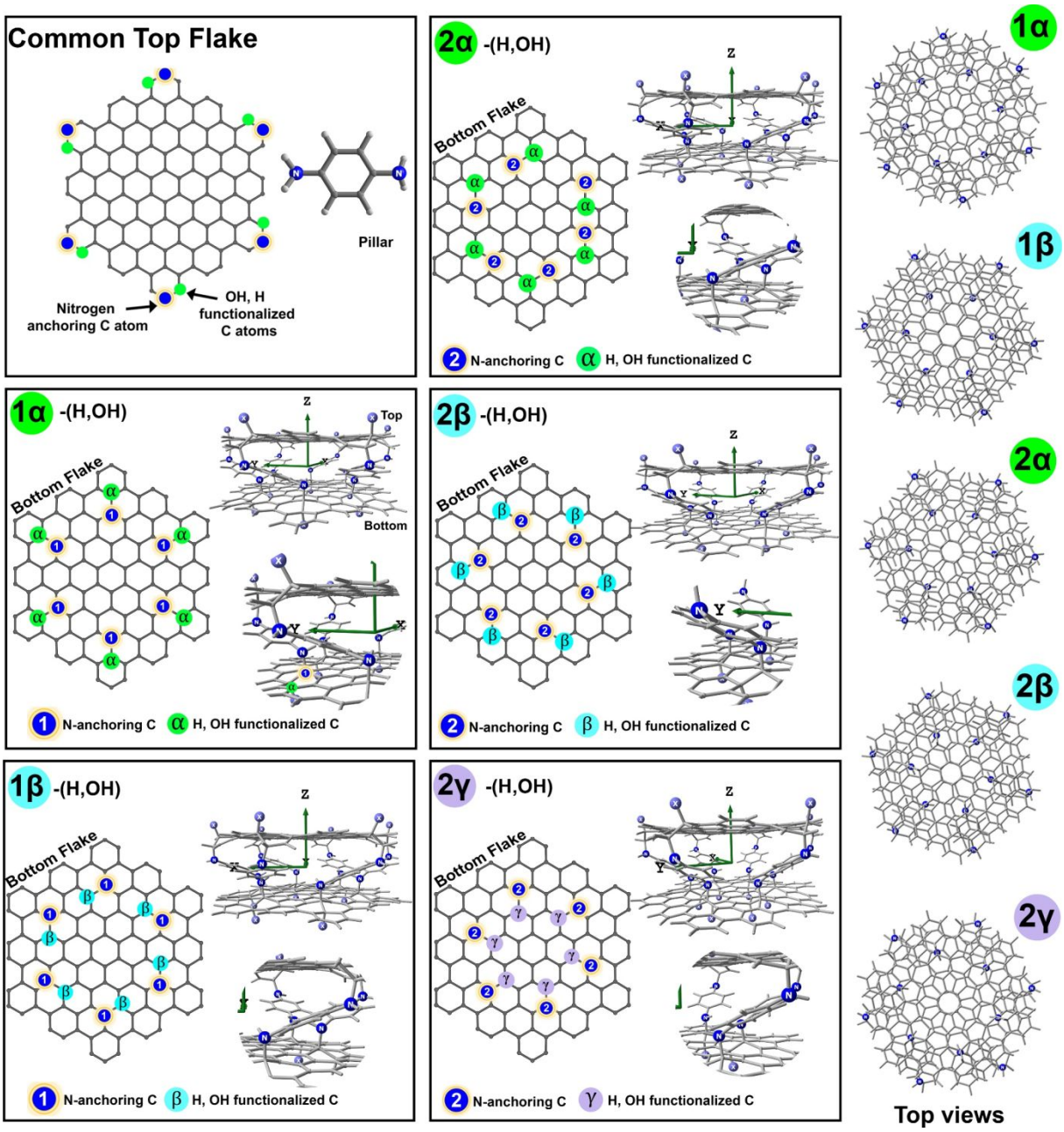

Figure 1. Nomenclatures of pillared graphene **flakes (PGFs)** and illustrations of the corresponding cross-linking patterns. All PGFs share the same top flake. Each PGF is named as a function to the cross-linking pattern of its bottom flake as (**1, 2**)**- (α, β, γ)** and with respect to the chosen functionalization with **(H, OH)**. Description: "**1**", "**2**" denote sp^3 hybridized C atoms of the bottom flakes bonded to one N atom of the p-diaminophenyl pillar at a specific position (**1**, **2**) as shown in the figure; "**α**," "**β**," and "**γ**" denote sp^3 hybridized C atoms of the bottom flakes functionalized with X= (H or OH) as shown in **Fig. 2.** Example: **1α-(OH)**: the nitrogen atom of the diamine pillar is bonded to the carbon atom "**1**", with a hydroxyl (**-OH)** bonded to the carbon atom at position "**α**."

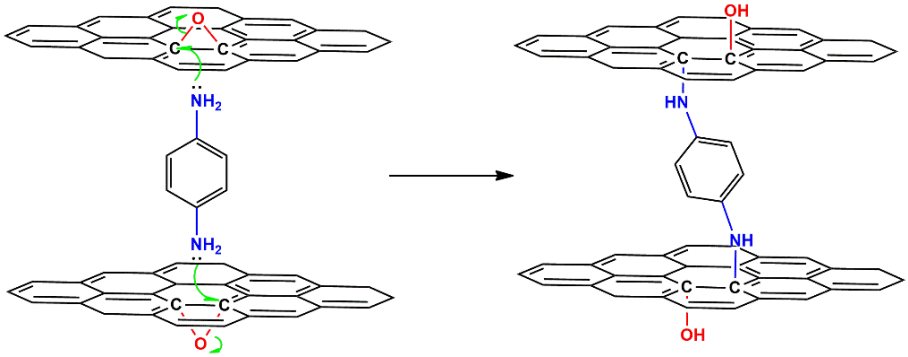

Figure 2. Schematic representation of S_N2 nucleophilic attack reaction between 1,4 benzenediamine and GO epoxides.

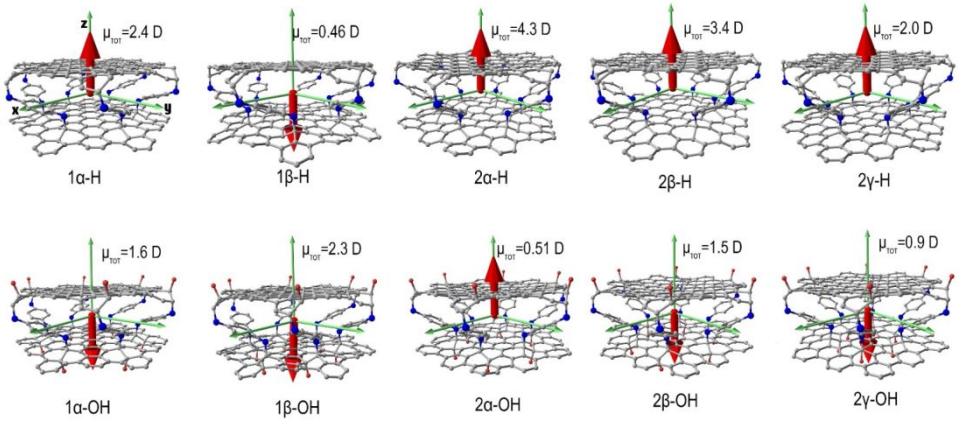

Figure 3. Dipole moment vectors (red arrows) and scalar t values (μ_{TOT}) are given in Debye (D) of all PGFs shown in Figure **1** **Hydrogen** atoms are not shown in this figure. Rows correspond to the same varying linking patterns **1α**, **1β**, etc. (see Figure **1**), and columns correspond to the same cross-linking pattern with different substitutions (X=H, OH). Cartesian axes in each case are given as green arrows. All computations have been performed at the CAM-B3LYP/def2-SVP level of theory on PBE0/def2-SVP optimized geometries of C_1 symmetry.

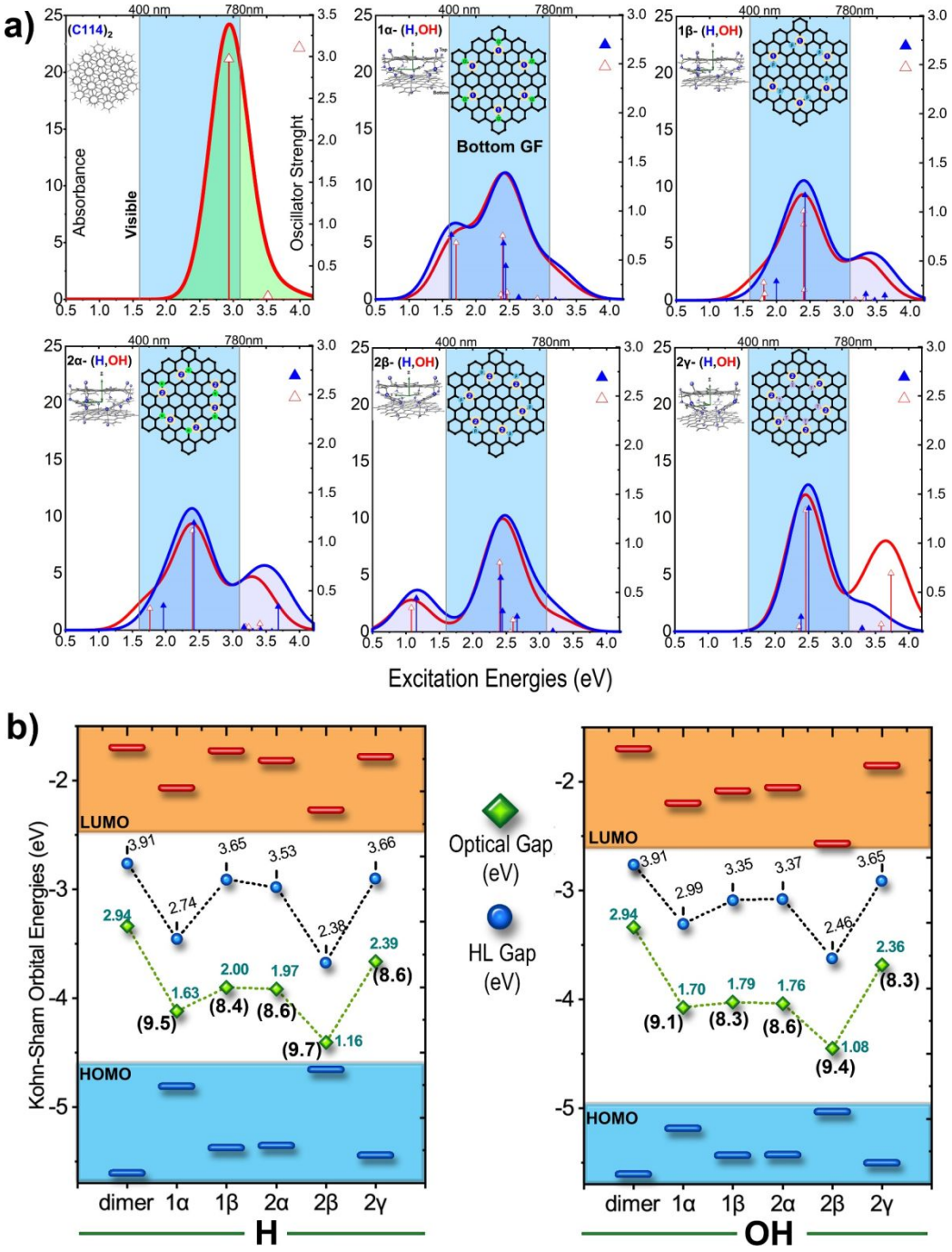

Figure 4 (**a**) UV-Vis simulated spectra of pillared graphene flakes interconnected with six 1,4- benzenediamine linkers computed at the TD-CAM-B3LYP/def2-SVP/ level. (**b**) Kohn-Sham orbital energies, HOMO-LUMO, and optical gaps (eV) of pillared graphene flakes interconnected with six 1,4- benzenediamine linkers. Values in parentheses correspond to the dipole polarizabilities per atom (au). All values have been computed at the CAM-B3LYP/def2-SVP level of theory.

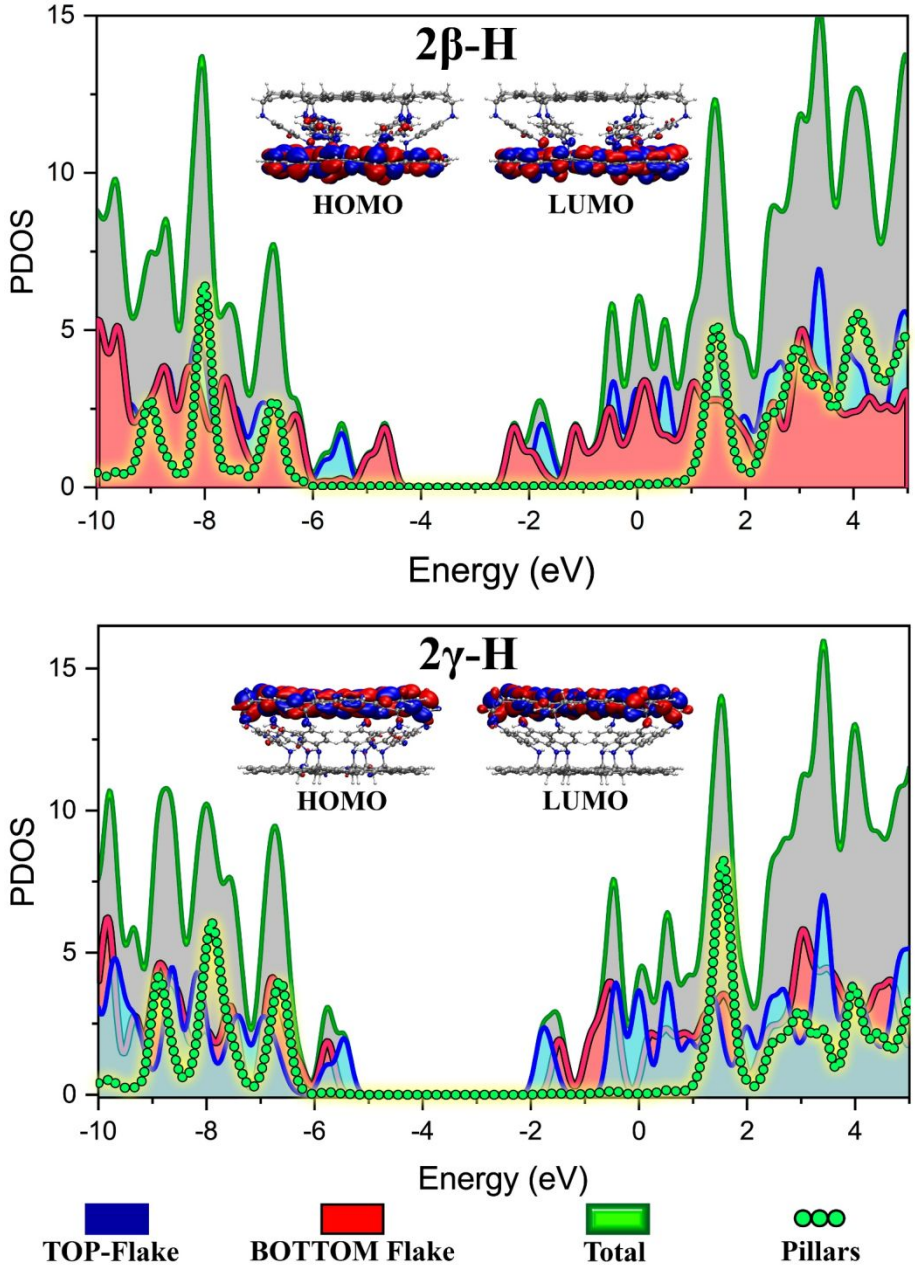

Figure 5. Projected density of states and HOMO-LUMO orbitals computed at the CAM-B3LYP/def2-SVP level of theory.

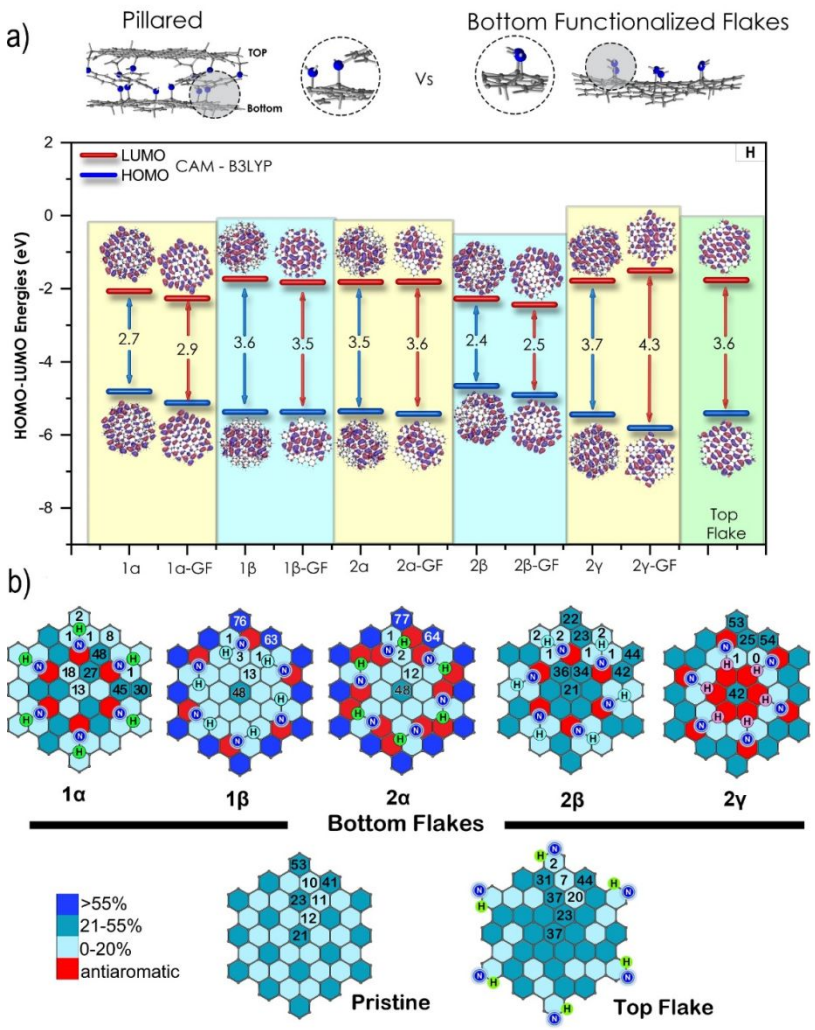

Figure 6. a) HOMO-LUMO gap comparisons between PGFs of in Fig. 1 and the corresponding non-pillared top flakes (designated with the extension -GF at the bottom axis). The isolated flakes have been functionalized with -NH_2 and -H, groups at the same atoms as in their pillared counterparts. All computations have been performed at the CAM-B3LYP/def-2SVP level of theory on PBE0/def2-SVP optimized geometries. **b)** CAM-B3LYP/def2-SVP π-delocalization patterns per carbon hexagon of the isolated bottom functionalized flakes of all PGFs. The delocalization values are given as percentage differences with respect to the isolated benzene molecule computed with the same method. For example, the π-electron delocalization in the three terminal axial-aromatic sextets of pristine C_{114} is 53% of the delocalization of C_6H_6 computed at the respective level of theory.

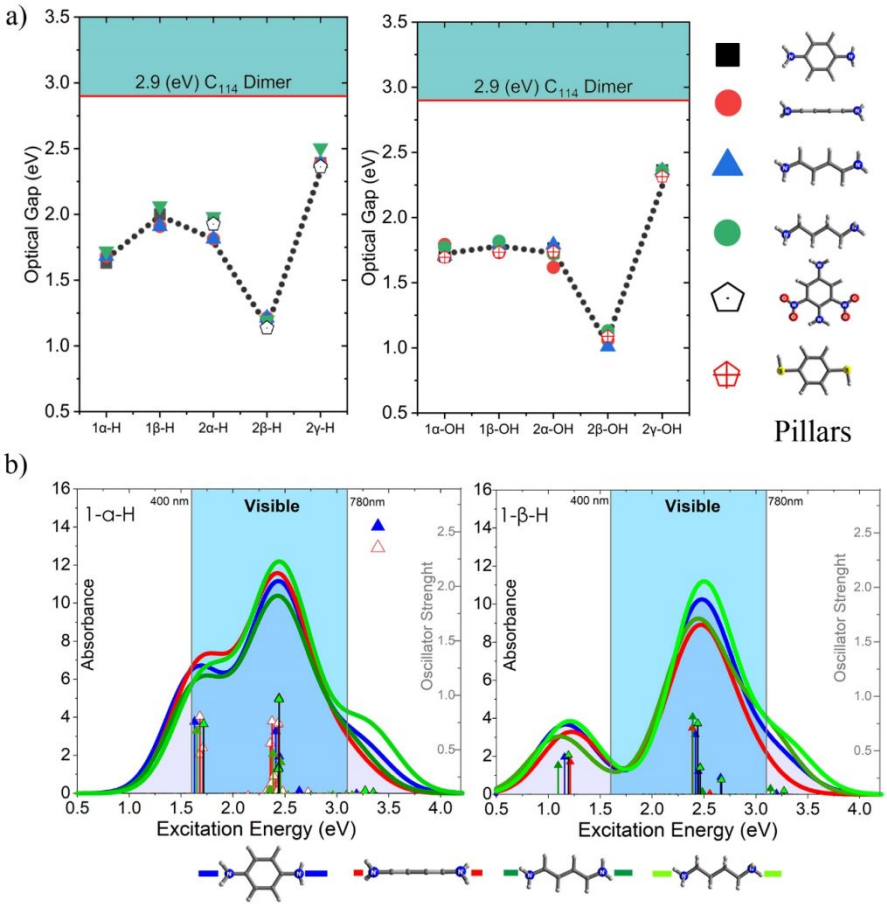

Figure 7. a) Optical gaps (energy difference between the ground electronic states and the first allowed by symmetry excited state) of PGFs interconnected with six pillars of a different character in terms of conjugation, polarity, and linking atom. b) UV-Vis simulated spectra (90 states) of PGFs interconnected by various diamine pillars. Each PGF is interconnected by six pillars of the same type. All computations have been performed within the Time-Dependent Density Functional framework by applying the CAM-B3LYP/def2-SVP basis set on PBE0/def2-SVP optimized geometries.

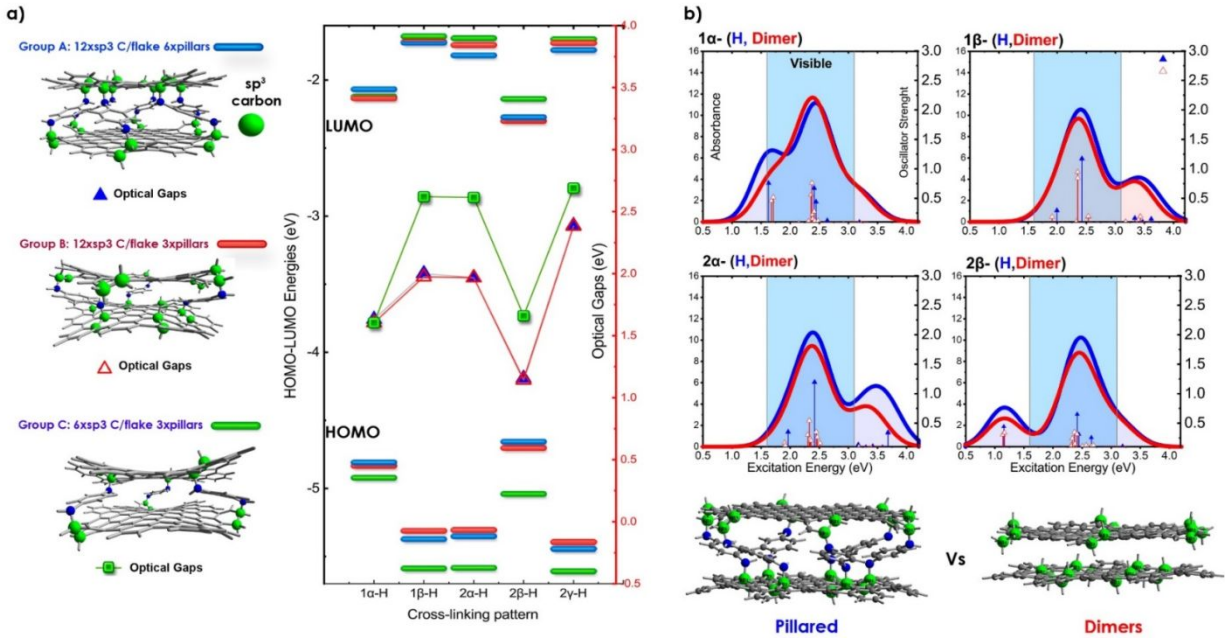

Figure 8. **a)** Optical gaps (and frontier orbital energies of PGFs interconnected with six and three pillars. Grey hexagons correspond to aromatic dark sextets. Group A comprises structures **2α, 2β**, and **2γ** -(H) containing twelve sp^3 atoms in each GF. Starting from group A, we constructed an additional group of models (group B) by removing three of the six pillars un each PGF. To maintain the sp^3 character of the corresponding binding carbon atoms, we added a hydrogen atom in each binding position. Finally, the third group (group C) has been built upon the structures of group B by converting the non-pillared sp^3 hybridized carbon atoms to sp^2. **b)** Comparison of UV-Vis spectra of the optical gap are defined as the energetic difference between the ground electronic states and the first allowed by symmetry excited state of each system. All computations have been performed within the Time-Dependent Density Functional framework by applying the long-range corrected CAM-B3LYP functional with the def2-SVP basis set on PBE0/def2-SVP fully optimized geometries.

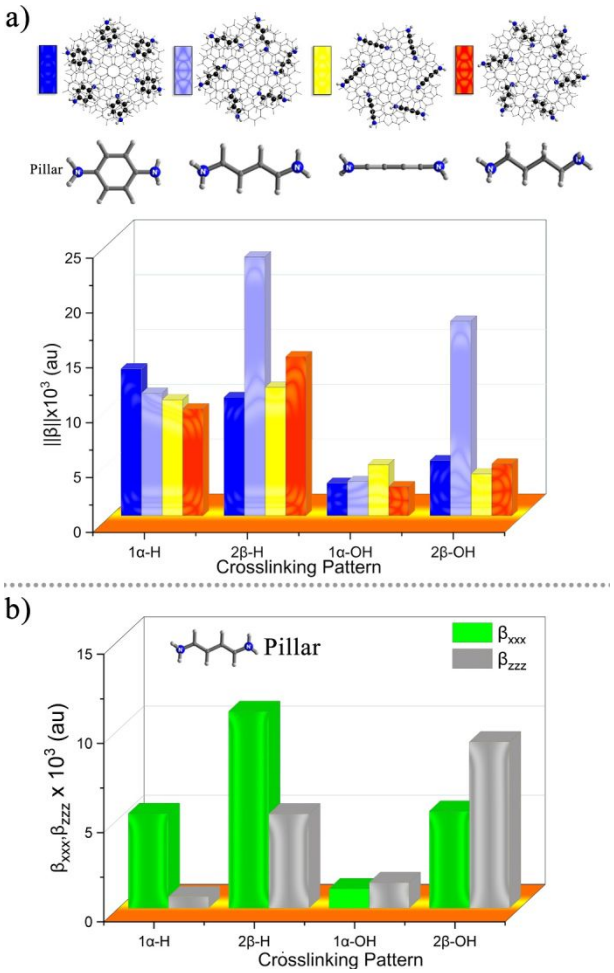

Figure 9. a) Pillar dependence of the first dipole hyperpolarizability modulus ||β||. **b)** Parallel (β_{xxx}) and perpendicular (β_{zzz}) to the graphene flake layers tensorial components of the first hyperpolarizability in the case of diamino-butadiene pillared species. All computations have been carried out with the long-range corrected functional CAM-B3LYP and the def2-SVP basis set on PBE0/def2-SVP optimized geometries with Grimme's D3 empirical dispersion.

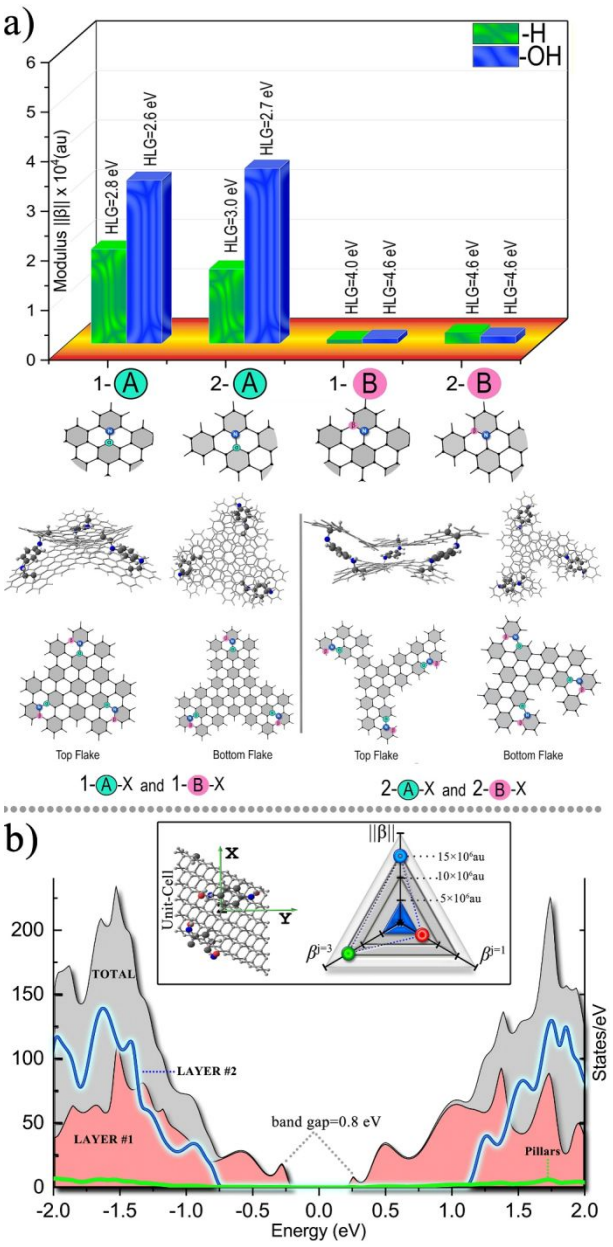

Figure 10. a) Cross-linking pattern dependence of the first dipole hyperpolarizability modulus $||\beta||$ in four pillared graphene flakes of large sizes. All computations have been carried out with the long-range corrected functional CAM-B3LYP and the def2-SVP basis set on PBE0/def2-SVP fully optimized geometries, including Grimme's D3 empirical dispersion. Grey-shaded carbon hexagons correspond to aromatic Clar sextets. All species have twelve sp^3 atoms equally distributed in each flake. In species denoted with the letter "**A,**" all sp^3 carbon atoms belong to two neighboring aromatic sextets of the pristine parent flake. On the other hand, in species denoted with the letter "**B**," all sp^3 carbon atoms reside in the same aromatic sextet of their parent pristine, isolated graphene flakes. **b)** Projected density of states and modulus ||β|| together with dipolar and octupolar contributions of a periodic graphene oxide bilayer slab interconnected by two diamino benzene pillars per unit cell computed at CAM-B3LYP/pob-DZVP-rev2 level of theory. The lattice of the system, built from 162 atoms in total, has been optimized at the PBE0/pob-DZVP-rev2 level of theory, including Grimme's D3 empirical dispersion.